Solubility measurements of refrigerants in polyolesters lubricants at temperature from 323K to 383K

Julien Brocus, Alain Valtz, Christophe Coquelet, Florence de Carlan

Solubility measurements of refrigerants in polyolesters lubricants at temperature from 323K to 383K.

Julien Brocus[a,b], Alain Valtz[a], Christophe Coquelet[a*], Florence De Carlan[b]

[a]Mines Paristech, PSL University, CTP – Centre of Thermodynamics and Processes, 35 rue Saint-Honoré, 77300 Fontainebleau, France.

[b] EDF LAB LES RENARDIERES – Centre R&D, Moret Loing et Orvanne, 77250, France.

*Corresponding author. E-mail address: christophe.coquelet@mines-paristech.fr. Telephone: +33164694962

Abstract

In refrigeration systems and heat pumps, lubricant selection is important to avoid issues that can lead to a breakdown of the compressor and the entire system. Daniel plots are a great tool to make the selection. Half of the graph is the solubility of refrigerant in lubricating oil. Isothermal vapor-liquid equilibrium (VLE) data are measured for five refrigerants in four oils. Refrigerants include HFC-32 (dichlorofluoromethane), HFC-134a (1,1,1,2-tetrafluoroethane), HFO-1234yf (2,3,3,3-tetrafluoropropene), HFO-1336mzz(Z) (cis-1,1,1,4,4,4-hexafluoro-2-butene) and HCFO-1233zd(E) (trans-1-chloro-3,3,3-trifluoroprop-1-ene) in four oils named POE 80, SE 55, SE 170 and SE 220, based on their viscosity grade. The experimental technique used is based on static synthetic methods. All of the data are correlated with the cubic equation of state developed by Yokozeki.

Keywords: refrigerants, lubricants, solubility, heat pumps.

Nomenclature

a	Energy parameter of the equation of state ($J.m^3.mol^{-2}$)	b	Molar covolume parameter of the equation of state ($m^3.mol^{-1}$)
F	Objective function	f_{ij}	Binary interaction parameter
k_{ij}	Binary interaction parameter	l_{ij}	Binary interaction parameter
l_{ji}	Binary interaction parameter	m_{ij}	Binary interaction parameter
n	Number of points	P	Pressure (Pa)
R	Molar gas constant (8.314472 $J.mol^{-1}.K^{-1}$)	T	Temperature (K)
U	Combined expanded uncertainty	u	Uncertainty
v	Molar volume ($m^3.mol^{-1}$)	w	Liquid mass fraction
x	Liquid molar fraction		

Greek letters

α	Temperature dependent terme	β	Parameter of the alpha function
ν	Kinematic viscosity	τ	Binary interaction parameter
ω	Acentric factor		

Subscripts

i,j	Molecular species	c	Critical property
cal	Calibration	calc	Calculated value
cell	Cell	exp	Experimental value
liq	Liquid	rep	Repeatability
vap	Vapor		

Abbreviations

AAD	Absolute average deviation	EoS	Equation of state
GWP	Global warming potential	HCFO	Hydrochlorofluoroolefin
HFC	Hydrofluorocarbon	HFO	Hydrofluoroolefin
MM	Molecular weight	SRK	Soave-Redlich-Kwong
VI	Viscosity index		

1. Introduction

Industrial heat pumps are a great way to exploit and valorize low temperature waste heat sources (van de Bor et al., 2015). The compressor is one key component of any heat pumps and its life expectancy is tied to its proper lubrication. Selection of lubricant for heat pump system is then determinant. The lubricant is responsible for the lubrication of the moving parts of the compressor. If not properly lubricated, a compressor's life span can be reduced because of premature wear (Kruse and Schroeder, 1985). For the compressor manufacturer, selection of the lubricant is primordial.

In most heat pump systems, the refrigerant comes into contact with the lubricating oil, forming a mixture that can lead to potential lubrication issues (Quiñones-Cisneros et al., 2005) such as a lower kinematic viscosity or liquid-liquid equilibrium phenomena. Formation of two distinct liquid phases in the carter of the compressor can make the lubrication of moving pieces difficult to control as there is an oil-rich and a refrigerant-rich phase. The former would be the only one suitable for the proper lubrication of the compressor. Overall, it is best to avoid formation of liquid-liquid equilibrium in the compressor temperature and pressure conditions.

Even with an efficient oil separator installed, part of the lubricant oil can migrate from the compressor to other parts of the system such as the evaporator, condenser, expansion device and piping. Oil return to the compressor must be ensured to avoid draining the compressor out of its lubricant. If the oil is miscible with the refrigerant, over the various temperatures and pressures in the heat pump cycle, it will naturally flow back to the compressor thanks to the refrigerant flow. However, phase separation, in the form of liquid-liquid-vapor or liquid-liquid equilibria can result in accumulation of oil inside the tubes of the heat exchangers, reducing heat transfer and the overall performances of the heat pump (Dang et al., 2012). In addition, forming two liquid phases in piping can also lead to accumulation and default in oil return (Youbi-Idrissi and Bonjour, 2008).

To avoid potential issue, it is best to avoid liquid-liquid and liquid-liquid-vapor equilibrium in heat pump systems. The miscibility between refrigerant and oil lubricant needs to be investigated as well as the refrigerant solubility in the oil in order to properly characterize the formed mixture. Hence, phase diagram of the refrigerant-lubricant mixture are needed.

The selection of the lubricant is highly dependent on the application, i.e the technology of the compressor, the refrigerant, and temperature and pressure conditions (Mang and Dresel, 2007). The compressor will determine the minimum value of the kinematic viscosity needed for a proper lubrication (Figure 1). It will also influence the temperature and pressure at which the refrigerant-lubricant mixture lubricates the compressor.

The selection of the lubricant oil is done studying Daniel plots (Figure 1). Daniel plots are tools designed to investigate the suitability of a lubricant for a specific refrigerant (Daniel et al., 1982). The bottom half of the diagram shows how much refrigerant is dissolved into the lubricating oil at saturation conditions (temperature and pressure). The upper half indicates the kinematic viscosity of the liquid mixture in the same operating conditions and previously determined composition.

For example, let's consider a scroll compressor with a kinematic viscosity limit of 10 mm²/s, using a HFC-134a refrigerant wit h a Reniso Triton SE55 lubricant. The Daniel plot of the refrigerant-lubricant mixture, provided in Figure 1, indicates that for working conditions of 60°C (333.15 K) and 4 bar (0.4 MPa), the liquid phase of the refrigerant-lubricant mixture is composed of 95% of lubricant, in mass (point A). This liquid phase have a kinematic viscosity of 16 mm²/s, which is higher than the minimum value tolerated by the compressor.

In most cases, these graphs are obtained after experimental work and measurement of solubility, density and dynamic viscosity of a refrigerant-oil lubricant binary. Correlations are then used to represent these measurements on Daniel plots. The objective of this work is to try to obtain Daniel plot with the use of thermodynamic models that could predict vapor-liquid equilibrium of these mixtures.

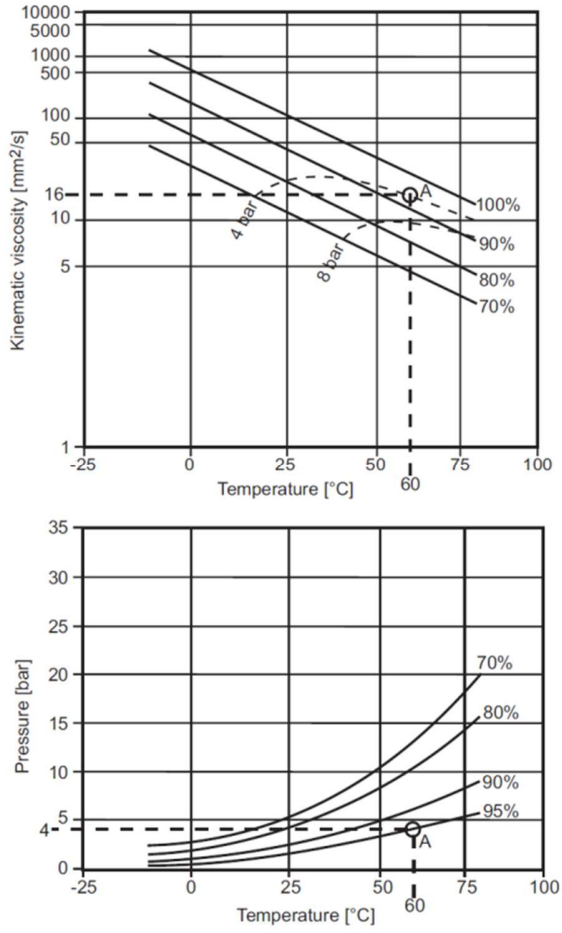

Figure 1 : Daniel plot of a RENISO Triton SE55-HFC134a mixture in lubricating oil composition (Mang and Dresel, 2007).

Modeling is useful to avoid extensive experimental studies which can be costly in resources and in time. Thermodynamic tools such as cubic equations of states can be used to predict the behavior and thermophysical properties for refrigerant- oil mixtures. Nonetheless, experimental work is always necessary to fit model parameters and for the validation of said models.

(Marsh and Kandil, 2002) provides a review of refrigerant-lubricant phase equilibrium data involving the most popular HFC such as HFC-32 and HFC-134a with, mostly, POE lubricants. It is noted that without structural information on the lubricants, it is difficult to provide a general prediction method to model refrigerant-lubricant mixtures phase diagrams or to allow comparison. Experimental data usually involves a pure oil component, with a detailed structure, or a commercially available lubricant more difficult to characterize. In the latter, oils are often named after their type and viscosity grade.

While HFO-lubricant phase equilibrium data are scarce, they are more numerous for refrigerant of interest such as HFO-1234yf. (Bobbo et al., 2014) studied the solubility of HFO-1234yf in two commercial PAG oils from 258K to 338K, even reporting liquid-liquid equilibria similar to the ones observed in this work. (Morais et al., 2020) investigated the mixture of HFO-1234yf in a POE lubricant from 248K to 348K, but not observing any partial immiscibility.

(Sun et al., 2017), (Sun et al., 2020), (Wang et al., 2016), studied the solubility of HFO-1234yf in several linear chained esters (PEC4 up to PEC9) with an isochoric saturation method from 293 to 348K. The purpose of these studies is to compare the solubility of the refrigerant according to the length of the linear chain of the lubricant. No immiscibility was observed.

(Jia et al., 2020) studied the solubility of HFO-1234yf in a commercial POE lubricant from 278 to 348K. (Jia et al., 2021) studied the solubility of HFO-1234yf in a POE, PVE and PAG commercial base oils from 273 to 353K. Both studies used the same isochoric saturation method from previous citations and no immiscibility was observed in the range of the studies. It is worth noting that (Jia et al., 2020) is the only paper referencing the different molecular component constituting the lubricant.

(Marcelino Neto et al., 2014) studied the phase diagram of HFO-1234yf and HFC-134a in a POE ISO VG 10 lubricant with a static synthetic method from 286 to 353K. No liquid-liquid equilibria was observed. Though, no numerical data are provided.

All of the previously cited literature report type III phase diagrams, according to the bon Konyneburg and Scott classification (Konynenburg and Scott, 1980). This is coherent with typical refrigerant-lubricant phase equilibria as explained by (Quiñones-Cisneros et al., 2005).

To our knowledge, there are no published experimental data of HFO-1336mzz(Z) and HCFO-1233zd(E) in lubricants.

This work provides liquid-vapor data of refrigerant-lubricant mixtures at temperatures from 323 K to 383 K using a static-synthetic method. They are correlated using an equation of state (EoS) based on Yokozeki's publications (Yokozeki, 2001), (Yokozeki, 2007). His model takes into account the difference in molecule size between refrigerants and lubricants. Moreover, liquid-liquid equilibria are usually well represented. The refrigerant studied are HFC-32 and HFC-134a, two widely used refrigerants, HFO-1234yf and HFO-1336mzz(Z) and an hydrochlorofluoroolefin (HCFO) HCFO-1233zd(E).

2. Experimental section

2.1. Materials

In Table 1 we list the suppliers of the refrigerants with associated purities. No further purification was performed on the refrigerants. HFC-32 (dichlorofluoromethane), HFC-134a (1,1,1,2-tetrafluoroethane),

HFO-1234yf (2,3,3,3-tetrafluoropropene), HFO-1336mzz(Z) (cis-1,1,1,4,4,4-hexafluoro-2-butene) and HCFO-1233zd(E) (trans-1-chloro-3,3,3-trifluoroprop-1-ene).

Table 1: Purities and suppliers of refrigerants.

ASHRAE name	Chemical name	CAS number	Purity	Analysis method	Supplier
HFC-32	Dichlorofluoromethane	75-10-5	99.95 (vol.%)	GC	Climalife
HFC-134a	1,1,1,2-tetrafluoroethane	811-97-2	99.50 (vol.%)	GC	Climalife
HFO-1234yf	2,3,3,3-tetrafluoropropene	754-12-1	> 99.50 (w.%)	GC	Climalife
HFO-1336mzz(Z)	cis-1,1,1,4,4,4-hexafluoro-2-butene	692-86-2	> 99.99 (vol.%)	GC	Chemours
HCFO-1233zd(E)	trans-1-chloro-3,3,3-trifluoroprop-1-ene	102687-65-0	93 (vol.%)	GC	Synquest

GC : Gas chromatograph

Lubricants used in this work are presented in Table 2 with their associated viscosity index (VI) and kinematic viscosity at 313.15 and 373.15K. These values can be used along with an Ubbelohde-Walther model to correlate kinematic viscosity with temperature (Seeton, 2006). Lubricants were carefully degassed before their uses.

Table 2: Properties and suppliers of lubricants.

Oil	VI	v, 313.15K ($mm^2.s^{-1}$)	v, 373.15K ($mm^2.s^{-1}$)	Supplier
SHC Gargoyle 80 POE	142	78	11.4	Mobil
Reniso Triton SE 55	137	55	8.8	Fuchs
Reniso Triton SE 170	111	173	17.6	Fuchs
Reniso Triton SE 220	98	220	19.0	Fuchs

2.2. Experimental apparatus

The apparatus used in this word, see Figure 2, is based on a static-synthetic method as described by (Descamps et al., 2005). The equilibrium cell is immersed in a thermo-regulated liquid bath (Lauda Proline RP 3530) which temperature is controlled within 0.01 K. The equilibrium cell (97 ± 3.9 cm^3 volume) composed of a sapphire tube pressed between two Hastelloy pieces, is identical to the cell used by (Zhang et al., 2016). The bottom flange holds a magnetic stirring assembly. In order to perform accurate measurement and to check for thermal gradients, two platinum resistance thermometers (Pt100 Ω) are inserted inside wells drilled in both flanges of the equilibrium cell and connected to a data acquisition unit (34972A LXI Data Acquisition Unit). These two Pt100 probes are periodically calibrated against a 25 Ω reference thermometer (Tinsley Precision Instrument) certified by the Laboratoire National d'Essais (LNE, Paris, France). The resulting accuracies on temperature measurements are within ±0.03 K. Pressures are measured by means of two pressure transducers (Druck PTX611, range 0-0.1 MPa and 0-5 MPa) connected as well to the acquisition unit. These transducers are calibrated with a modular pressure

controller (PACE 5000). The resulting accuracies in pressure measurements are within ±0.0003 MPa. Refrigerant and lubricant oil are charged into the cell with two variable volume cylinders (55.03 cm and 40.02 cm diameters) connected to an opto-electronic displacement transducer and a pressurizing circuit (nitrogen). Each variable volume cylinder has its own pressure transducer and a platinum resistance thermometer.

Uncertainties of pressure and temperature are calculated so that:

$$u(P) = \sqrt{u^2{}_{rep}(P) + u^2{}_{cal}(P)} \quad (1)$$

$$u(T) = \sqrt{u^2_{rep}(T) + u^2_{cal}(T)} \quad (2)$$

With the type B uncertainty (*GUM*, 2008) :

$$u_{cal}(P) = \frac{\max(\Delta P)}{\sqrt{3}} \quad (3)$$

$$u_{cal}(T) = \frac{\max(\Delta T)}{\sqrt{3}} \quad (4)$$

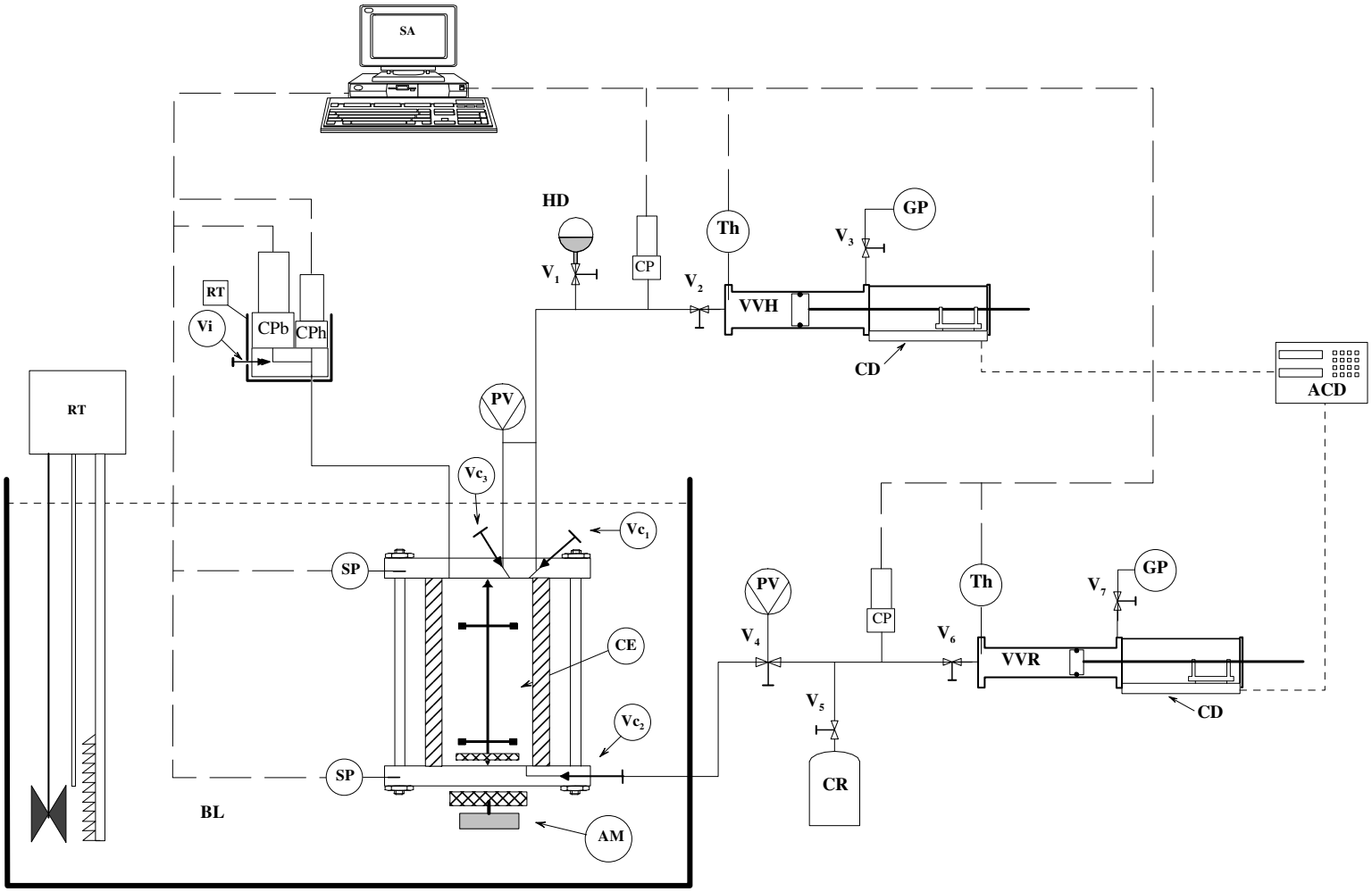

Figure 2 : Schematic Apparatus description. RT: Temperature Control; CPb, CPh : Pressure Transducers (Low and High pressure); Vi :Valves; Vci : Loading valves; PV : Vacuum pump; BL : Liquid Bath; SP : Platinum probes; CE : Equilibrium cell; AM : Magnetic stirrer; CR : Refrigerant cylinder; Th : Thermocouple; GP : Pressurizing gas; CD : Displacement transducer: VVR : Variable Volume cell for Refrigerant; VVH : Variable Volume cell for Oil; HD : Degassed Oil; ACD : Displacement acquisition unit; SA : Acquisition unit system.

2.3. Experimental procedure

The experimental procedure for the static-synthetic method, consists in the introduction of known amount of degassed lubricant oil and refrigerant in the thermostated system. First, the cell, loading and circuit lines are evacuated down to 0.1 Pa using the vacuum pump (see figure 2). The system is then thermostated at the desired temperature. The degassed lubricant oil is introduced into the equilibrium cell through the loading lines and the variable volume cell (VVH). The displacement of the piston (contained in the variable volume cylinder) and the pressure and temperature of the variable volume cell are recorded. After measurement of the lubricant vapour pressure and the level of the liquid phase, refrigerant is introduced from another variable volume cell (VVR). In order to have the best accuracy for the estimation of quantity of refrigerant loaded, pressure and temperature of VVR are recorded before and after each loading. The system is agitated until the pressure becomes stable, indicating that an equilibrium is reached. The values of pressure and temperature are recorded. The level of the liquid phase is measured with a graduated ruler (graduation down to 0.5mm). In order to complete the phase diagram, refrigerant is added into the cell and the procedure is repeated.

Vapor pressures of lubricating oil are so low compared to those of the refrigerants that oil is essentially non-present in the vapor phase. It makes static synthetic methods particularly suited for the measurement of vapor-liquid equilibria of refrigerant-lubricant mixtures as it simplifies the mass balance. The solubility is computed as the mass or molar fraction of refrigerant in the liquid phase. The mass fraction of refrigerant (Equation (5)) of the liquid phase is calculated thanks to the total mass of refrigerant introduced (m_i^{tot}) and the residual mass in the vapor phase (m_i^{vap}), as well as with the mass of oil introduced (m_{oil}).

$$w_i = \frac{m_i^{tot} - m_i^{vap}}{(m_i^{tot} - m_i^{vap}) + m_{oil}} \quad (5)$$

Where the mass of refrigerant and oil introduced with the variable volume cell are calculated with equations (6 - 7):

$$m = V \times \rho \quad (6)$$

$$V = \frac{\pi D^2}{4}\left(l_f - l_i\right) \quad (7)$$

V is the volume displaced by the piston, D is the diameter of the variable volume cell, (l_f-l_i) is the distance moved by the piston. Density of the refrigerant is computed with REFPROP 10.0 (Lemmon et al., 2018) as a function of temperature and pressure Density of the oil is calculated with equations (8 - 9).

$$\rho = A\bar{T} + B \quad (8)$$

$$\bar{T} = \frac{T_f + T_i}{2} \quad (9)$$

A and B are two parameters fitted beforehand for each oil on experimental data determined using a vibrating tube densitometer. $\bar{T}$ is the mean temperature measured during the introduction of oil in the equilibrium cell. The residual mass of refrigerant in the vapor phase is calculated with equation (6) with the volume of the vapor phase calculated using Equation (10).

$$V_{vap} = V_{cell} - V_{liq} \quad (10)$$

The cell volume has been determined after calibration. The liquid volume has been calculated with the measured height of liquid in the equilibrium cell and the inner diameter of the equilibrium cell (volume of the stirrer is taken into account). To obtain mole fraction from mass fraction we use Equation (11).

$$x_i = \frac{{w_i}/{M_i}}{{w_i}/{M_i} + {(1-w_i)}/{M_j}} \quad (11)$$

M_i is the molecular weight of the refrigerant and M_j the molecular mass of the oil (taken as 550 g.mol^{-1} for all the oils). Uncertainties associated with these calculations are detailed in the appendix.

3. Modeling

The experimental VLE data are correlated using a SRK-type cubic equation of state (Soave, 1972), (Redlich and Kwong, 1949), shown in equation (12):

$$P = \frac{RT}{v-b} - \frac{a(T)}{v(v+b)} \quad (12)$$

The attractive term a and the co-volume b, are respectively given by equations (13) and (14), while mixture parameters are obtained from equations (15) and (16), as described by (Yokozeki, 2007). Where f_{ij} is a function of temperature and the k_{ij} form is the result of size difference between refrigerant and oil molecules as discussed in (Yokozeki, 2001).

$$a = \sum_{i,j=1}^{C} \sqrt{a_i a_j} f_{ij}(T)\left(1 - k_{ij}\right) x_i x_j \quad (13)$$

$$b = \frac{1}{2}\sum_{i,j=1}^{C}\left(b_i + b_j\right)\left(1 - m_{ij}\right)\left(1 - k_{ij}\right)x_i x_j \quad (14)$$

$$f_{ij}(T) = \tau 0_{ij} + \frac{\tau 1_{ij}}{T} + \tau 2_{ij} T, \ where\ f_{ij} = f_{ji}\ et\ f_{ii} = 1 \quad (15)$$

$$k_{ij} = \frac{l_{ij} l_{ji}(x_i + x_j)}{l_{ji} x_i + l_{ij} x_j}, \ where\ \ k_{ij} = k_{ji}\ et\ k_{ii} = 0 \quad (16)$$

Where $m_{ij} = m_{ji}$ and $m_{ii} = 0$.
In this model, there are up to six interaction parameters for each binary pair: l_{ij}, l_{ji}, m_{ij}, $t_{0,ij}$, $\tau_{1,ij}$, $\tau_{2,ij}$. When $l_{ij} = l_{ji}$ in equation (16) and $f_{ij} = 1$, equation (13) becomes the classical quadratic mixing rule. The mixing rule used here can be regarded as a modified van der Waals-Berthelot mixing formula as described by Yokozeki (Yokozeki, 2001).

The pure component parameters are calculated with equations (17) and (18). Only a slight change has been made from the original paper of Yokozeki (2001), on the α function. As shown by equations (19) and (20), the first parameter β_0 should not be fitted, but taken as a constant equal to 1 in order to fit the requirements of an α function (Coquelet et al., 2004), (Le Guennec et al., 2016). In this case, for Tr equal to unity, the alpha function should exactly be equal to one.

$$a_i = 0.427480 \frac{\left(RT_{c,i}\right)^2}{P_{c,i}} \alpha_i(T) \quad (17)$$

$$b_i = 0.08664 \frac{RT_{c,i}}{P_{c,i}} \quad (18)$$

And α(T) is given by:

$$\alpha(T) = \sum_{k=0}^{\leq 3} \beta_k (1/T_r - T_r)^k, \quad for\ T_r \equiv T/T_c \leq 1 \tag{19}$$

$$\alpha(T) = \beta_0 + \beta_1 [exp\{2(1 - T_r)\} - 1], \quad for\ T_r \geq 1 \tag{20}$$

Where β_k are adjustable parameters calculated so as to reproduce pure component vapor pressure. They are adjusted on literature data for the whole temperature domain (323K to 383K) using a modified simplex algorithm by (Nelder and Mead, 1965) which objective function is defined by:

$$F = \frac{100}{N} \sum \left(\frac{P_{exp} - P_{calc}}{P_{exp}} \right)^2 \tag{21}$$

Where N is the number of data points, P_{exp} is the measured pressure, and P_{calc} is the calculated pressure.

Binary interaction parameters (m_{ij}, l_{ij}, l_{ji} and f_{ij}) were adjusted on experimental data with the same procedure, using the objective function defined by eq. 22.

$$F = \frac{100}{N} \sum \left(\frac{P_{exp} - P_{calc}}{P_{exp}} \right)^2 \tag{22}$$

4. Results

4.1. Pure components

Table 3 presents critical temperature and pressure, as well as acentric factors for all considered refrigerants and oils. For the oils we have used the recommended values suggested by Yokozeki (2001). Table 4 presents pure component parameters β_k, calculated so as to reproduce experimental vapor pressures. We used data from (Malbrunot et al., 1968) for HFC-32 (AAD: 0.3%, BIAS: -0.1%), (Baehr and Tillner-Roth, 1991) for HFC-134a (AAD: 0.7%, BIAS: -0.7%), (Richter et al., 2011) for HFO-1234yf (AAD: 0.1%, BIAS: -0.04%), (Tanaka et al., 2016) for HFO-1336mzz(Z) (AAD: 0.08, BIAS: 0.02%) and (Mondéjar et al., 2015) for HCFO-1233zd(E) (AAD: 0.2%, BIAS: -0.07%). We can observe that the deviations are less than 1%. We used a single set of parameters to calculate the vapor pressure of all the oils, as proposed by Yokozeki (Yokozeki, 2001). Although, in his work, Yokozeki suggests that the β_1 parameter of the oil should be treated as an adjustable parameter we chose to fix it at 1.0 so as not to add another adjustable parameter and because of a lack of vapor pressure measurement for the oil. Though, in his work, no acentric factor was provided, we used the value of a long chain hydrocarbon, the n-eicosane (Liu and Chen, 1996).

Table 3 : Critical parameters and acentric factors of refrigerants (REFPROP 10.0) and oils.

Component	Tc (K)	Pc (MPa)	ω	MM (g.mol^{-1})
HFC-32	351.26	5.7820	0.2769	52.024
HFC-134a	374.21	4.0593	0.32684	102.03
HFO-1234yf	367.85	3.3822	0.276	114.04
HFO-1336mzz(Z)	444.50	2.9030	0.386	164.06
HCFO-1233zd(E)	439.30	3.6237	0.3025	130.5
Oils	800	0.95	0.907	550

Table 4 : β_k parameters of the α(T) function.

Component	β1	β2	β3	AAD (%)	BIAS (%)
HFC-32	0.492992	-0.0901365	0.0130446	0.3	-0.1
HFC-134a	0.551218	-0.24555	0.242884	0.7	-0.7
HFO-1234yf	0.489753	-0.0979593	0.0274797	0.1	-0.04
HFO-1336mzz(Z)	0.589525	-0.184949	0.12507	0.08	0.02
HCFO-1233zd(E)	0.517259	-0.120512	0.0426607	0.2	-0.07
Oils	1.0	/	/	/	/

4.2. Mixtures

Experimental results are presented in Tables 5 to 14 and plotted on figures 3 to 12. Combined expanded uncertainties on pressure, temperature and composition (mass fraction w_i and molar fraction x_i) are also displayed in the tables of results. The results of modeling using Yokozeki's model are also presented in Tables 5 to 14. We have also indicated the liquid-liquid equilibria region on the figures (it was realized graphically). Table 15 presents the binary interaction parameters for each binary and each temperature, as well as mean BIAS, mean absolute deviation (calculated from equations 23 and 24) and absolute difference between measured and calculated pressure at the same composition (ΔP):

$$AAD(\%) = \frac{100}{N}\sum\frac{|X_{calc}-X_{exp}|}{X_{exp}} \quad (23)$$

$$BIAS(\%) = \frac{100}{N}\sum\frac{X_{calc}-X_{exp}}{X_{exp}} \quad (24)$$

Table 5 : Liquid-vapor data of HFC-32 – POE 80 system at 333 K and 343 K.

Experimental data					Calculated data	
P_{exp} *MPa*	$w_{ref, exp}$	$x_{ref, exp}$	u(w, k = 2)	u(x, k = 2)	P_{calc} *MPa*	ΔP *MPa*
T = 333.16 K						
0.1392	0.00949	0.0920	0.0008	0.007	0.1751	0.036
0.4240	0.0282	0.235	0.003	0.02	0.4172	0.0067
0.7792	0.0533	0.373	0.005	0.02	0.7047	0.074
1.1729	0.0829	0.489	0.007	0.02	1.0582	0.11
1.5312	0.111	0.569	0.009	0.02	1.4052	0.13
1.9334	0.145	0.642	0.01	0.02	1.8245	0.11
2.3515	0.185	0.705	0.01	0.02	2.2857	0.066
2.7513	0.228	0.758	0.01	0.02	2.7355	0.016
3.1375	0.275	0.800	0.02	0.01	3.1290	0.0085
3.4870	0.325	0.836	0.02	0.01	3.4588	0.028
T = 343.12 K						
0.1374	0.00472	0.0478	0.0008	0.007	0.1343	0.0031
0.5215	0.0255	0.217	0.003	0.02	0.5447	0.023
0.9438	0.0493	0.354	0.006	0.03	0.9309	0.013
1.4137	0.0762	0.466	0.008	0.03	1.3743	0.039
1.9438	0.109	0.564	0.01	0.03	1.9351	0.0087
2.5951	0.148	0.648	0.02	0.03	2.6010	0.0059
3.2408	0.194	0.718	0.02	0.02	3.3271	0.086
3.9696	0.237	0.766	0.02	0.02	3.9285	0.041

U(T, k = 2) = 0.003 K, U(P, k = 2) = 0.0001 MPa

Table 6 : Liquid-vapor data of HFC-32 – SE 55 mixture at 323K and 333K.

Experimental data					Calculated data	
P_{exp} *MPa*	$w_{ref, exp}$	$x_{ref, exp}$	u(w, k = 2)	u(x, k = 2)	P_{calc} *MPa*	ΔP *MPa*
T = 323.02 K						
0.0712	0.00389	0.0397	0.0005	0.005	0.0700	0.0012
0.3024	0.0214	0.188	0.002	0.01	0.3129	0.010
0.5995	0.0448	0.332	0.004	0.02	0.5935	0.0060
0.9706	0.0753	0.463	0.006	0.02	0.9598	0.011
1.2609	0.100	0.541	0.008	0.02	1.2578	0.0031
1.5603	0.124	0.600	0.009	0.02	1.5353	0.025
2.0805	0.180	0.699	0.01	0.02	2.1055	0.025
2.4573	0.230	0.759	0.02	0.02	2.4925	0.035
2.7496	0.277	0.802	0.02	0.01	2.7659	0.016
3.0329	0.338	0.844	0.02	0.01	2.9906	0.042
T = 333.00 K						
0.0912	0.00211	0.0218	0.0006	0.006	0.0505	0.041
0.4655	0.0247	0.211	0.003	0.02	0.4615	0.0041
1.0663	0.0647	0.422	0.008	0.03	1.0849	0.019
1.5571	0.100	0.541	0.01	0.03	1.6402	0.083
2.0044	0.134	0.620	0.01	0.03	2.1300	0.13
2.3722	0.160	0.669	0.01	0.02	2.4938	0.12
2.9059	0.212	0.740	0.02	0.02	3.0841	0.18
3.6177	0.289	0.811	0.03	0.02	3.6934	0.076

U(T, k = 2) = 0.003 K, U(P, k = 2) = 0.0001 MPa

Table 7 : Liquid-vapor data of HFC-32 – SE 170 mixture at 333K and 343K.

Experimental data					Calculated data	
P_{exp} *MPa*	$w_{ref, exp}$	$x_{ref, exp}$	u(w, k = 2)	u(x, k = 2)	P_{calc} *MPa*	ΔP *MPa*
T = 333.16 K						
0.0881	0.00352	0.0360	0.0005	0.005	0.0870	0.0010
0.2096	0.00930	0.0903	0.001	0.01	0.2127	0.0031
0.5120	0.0260	0.220	0.003	0.02	0.5164	0.0044
0.9440	0.0510	0.362	0.006	0.03	0.9229	0.021
1.4503	0.0844	0.493	0.009	0.03	1.4434	0.0070
1.9830	0.123	0.597	0.01	0.03	2.0033	0.020
2.6043	0.175	0.692	0.02	0.03	2.6531	0.049
3.3485	0.258	0.786	0.03	0.02	3.3859	0.037
3.8685	0.357	0.854	0.03	0.02	3.8440	0.024
T = 343.16 K						
0.0866	0.00274	0.0282	0.0005	0.005	0.0796	0.0070
0.3129	0.0135	0.126	0.002	0.02	0.3438	0.031
0.8602	0.0409	0.311	0.006	0.03	0.8943	0.034
1.6453	0.0827	0.488	0.01	0.04	1.6690	0.024
2.5586	0.138	0.629	0.02	0.04	2.6107	0.052
3.5932	0.196	0.721	0.03	0.04	3.4190	0.17
4.5143	0.297	0.817	0.04	0.03	4.3810	0.13

U(T, k = 2) = 0.003 K, U(P, k = 2) = 0.0001 MPa

Table 8 : Liquid-vapor data of HFC-134a – POE 80 mixture at 333K and 343K.

Experimental data					Calculated data	
P_{exp} *MPa*	$w_{ref, exp}$	$x_{ref, exp}$	u(w, k = 2)	u(x, k = 2)	P_{calc} *MPa*	ΔP *MPa*
T = 333.16 K						
0.0438	0.00605	0.0318	0.0005	0.003	0.4322	0.00055
0.1670	0.0266	0.128	0.002	0.008	1.6827	0.0012
0.3463	0.0612	0.260	0.004	0.01	3.5143	0.0051
0.5262	0.0966	0.366	0.006	0.02	5.3496	0.0087
0.7092	0.131	0.447	0.007	0.02	7.1332	0.0041
0.9282	0.165	0.516	0.009	0.02	8.9290	0.035
1.1263	0.203	0.579	0.01	0.02	10.8509	0.041
1.3376	0.270	0.666	0.01	0.01	13.7833	0.041
1.5750	0.331	0.728	0.01	0.01	15.8746	0.012
T = 343.17 K						
0.0700	0.0101	0.0520	0.0008	0.004	0.0743	0.0043
0.1822	0.0267	0.129	0.002	0.009	0.1811	0.0011
0.3511	0.0516	0.227	0.004	0.01	0.3252	0.026
0.5949	0.0913	0.351	0.006	0.02	0.5493	0.046
0.8624	0.139	0.464	0.009	0.02	0.8216	0.041
1.1562	0.196	0.569	0.01	0.02	1.1525	0.0037
1.4389	0.262	0.657	0.01	0.02	1.4967	0.058
1.6923	0.336	0.731	0.02	0.01	1.8048	0.11
1.9522	0.424	0.799	0.02	0.01	2.0779	0.096

U(T, k = 2) = 0.003 K, U(P, k = 2) = 0.0001 MPa

Table 9 : Liquid-vapor data of HFC-134a – SE 55 mixture at 323K and 343K

Experimental data					Calculated	
P_{exp} *MPa*	$w_{ref, exp}$	$x_{ref, exp}$	u(w, k = 2)	u(x, k = 2)	P_{calc} *MPa*	ΔP *MPa*
T = 323.02 K						
0.0583	0.0118	0.0605	0.0007	0.003	0.0593	0.010
0.1842	0.0370	0.171	0.002	0.009	0.1786	0.056
0.3407	0.0724	0.296	0.004	0.01	0.3410	0.0034
0.5027	0.109	0.398	0.006	0.01	0.5065	0.037
0.7571	0.172	0.528	0.009	0.02	0.7662	0.091
1.0023	0.244	0.634	0.01	0.01	1.0077	0.054
1.1896	0.311	0.708	0.01	0.01	1.1709	0.19
T = 343.02 K						
0.0666	0.00633	0.0332	0.0008	0.004	0.0497	0.017
0.3269	0.0415	0.189	0.005	0.02	0.3090	0.018
0.5292	0.0720	0.295	0.007	0.02	0.5242	0.0050
0.7289	0.102	0.380	0.009	0.02	0.7320	0.0031
0.9186	0.133	0.452	0.01	0.02	0.9397	0.021
1.1328	0.171	0.527	0.01	0.02	1.1837	0.051
1.3596	0.217	0.599	0.01	0.02	1.4412	0.082
1.5747	0.266	0.661	0.02	0.02	1.6766	0.10
1.8019	0.328	0.725	0.02	0.02	1.9074	0.11
2.0465	0.418	0.794	0.02	0.01	2.1027	0.056

U(T, k = 2) = 0.003 K, U(P, k = 2) = 0.0001 MPa

Table 10 : Liquid-vapor data of HFO-1234yf – POE 80 mixture at 333K and 343K.

Experimental data					Calculated data	
P_{exp} *MPa*	$w_{ref, exp}$	$x_{ref, exp}$	u(w, k = 2)	u(x, k = 2)	P_{calc} *MPa*	ΔP *MPa*
T = 333.16 K						
0.0726	0.00991	0.0460	0.0009	0.004	0.0733	0.00077
0.1827	0.0245	0.108	0.002	0.009	0.1806	0.0021
0.3317	0.0456	0.187	0.004	0.01	0.3300	0.0017
0.5436	0.0781	0.290	0.007	0.02	0.5447	0.0011
0.7735	0.118	0.391	0.01	0.02	0.7757	0.0023
1.0216	0.169	0.496	0.01	0.02	1.0256	0.0040
1.2179	0.220	0.576	0.01	0.02	1.2178	0.00013
1.3985	0.285	0.658	0.02	0.02	1.3982	0.00031
1.5711	0.391	0.756	0.02	0.02	1.5649	0.0062
T = 343.16 K						
0.0885	0.0106	0.0490	0.001	0.005	0.0945	0.0060
0.1977	0.0227	0.101	0.002	0.01	0.2022	0.0045
0.3915	0.0451	0.185	0.005	0.02	0.3943	0.0028
0.6555	0.0779	0.289	0.008	0.02	0.6571	0.0015
0.9502	0.117	0.390	0.01	0.03	0.9392	0.011
1.2679	0.168	0.493	0.02	0.03	1.2467	0.021
1.5449	0.223	0.581	0.02	0.03	1.5129	0.032
1.8169	0.294	0.668	0.02	0.02	1.7615	0.055
2.0299	0.373	0.742	0.02	0.02	1.9354	0.095

U(T, k = 2) = 0.003 K, U(P, k = 2) = 0.0001 MPa

Table 11 : Liquid-vapor data of HFO-1234yf – SE 55 mixture at 323K, 333K and 343K.

Experimental data					Calculated data	
P_{exp} *MPa*	$w_{ref, exp}$	$x_{ref, exp}$	u(w, k = 2)	u(x, k = 2)	P_{calc} *MPa*	ΔP *MPa*
T = 323.18 K						
0.0476	0.00520	0.0246	0.006	0.003	0.0378	0.010
0.1110	0.0142	0.0651	0.001	0.006	0.0961	0.015
0.2377	0.0349	0.148	0.003	0.01	0.2105	0.027
0.4177	0.0670	0.257	0.006	0.02	0.3705	0.047
0.6327	0.111	0.376	0.009	0.02	0.5853	0.047
0.8844	0.176	0.508	0.01	0.02	0.8874	0.0030
1.1040	0.259	0.628	0.02	0.02	1.2061	0.10
1.2237	0.334	0.708	0.02	0.01	1.3965	0.17
1.2892	0.420	0.777	0.02	0.01	1.4929	0.20
1.3008	0.485	0.820	0.02	0.009	1.5002	0.20
1.3013	0.534	0.847	0.01	0.007	1.4819	0.18
1.3018	0.576	0.867	0.01	0.006	1.4572	0.16
1.3020	0.611	0.884	0.01	0.005	1.4323	0.13
T = 333.00 K						
0.0871	0.00933	0.0435	0.001	0.005	0.0899	0.0028
0.2128	0.0265	0.116	0.003	0.01	0.2294	0.017
0.3704	0.0483	0.197	0.005	0.02	0.3859	0.015
0.5601	0.0743	0.279	0.007	0.02	0.5634	0.0033
0.7667	0.104	0.359	0.009	0.02	0.7629	0.0038
1.0585	0.127	0.412	0.01	0.03	0.9161	0.14
1.4022	0.177	0.508	0.02	0.03	1.2380	0.16
0.0871	0.00933	0.0435	0.001	0.005	0.0899	0.0028
T = 343.02 K						
0.0859	0.00753	0.0353	0.001	0.005	0.0843	0.0016
0.2150	0.0214	0.0955	0.003	0.01	0.2197	0.0047
0.4163	0.0449	0.185	0.005	0.02	0.4202	0.0040
0.6198	0.0699	0.266	0.008	0.02	0.6220	0.0022
0.8227	0.0955	0.337	0.01	0.03	0.8259	0.0032
1.0526	0.122	0.401	0.01	0.03	1.0349	0.018
1.3168	0.153	0.465	0.02	0.03	1.2786	0.038
1.6374	0.204	0.553	0.02	0.03	1.6670	0.030
1.9078	0.241	0.604	0.02	0.03	1.9180	0.010

U(T, k = 2) = 0.003 K, U(P, k = 2) = 0.0001 MPa

Table 12 : Liquid-vapor data of HFO-1234yf – SE 170 mixture at 333K and 343K.

Experimental data					Calculated data	
P_{exp} *MPa*	$w_{ref, exp}$	$x_{ref, exp}$	u(w, k = 2)	u(x, k = 2)	P_{calc} *MPa*	ΔP *MPa*
T = 333.17 K						
0.0822	0.00922	0.0429	0.001	0.005	0.0844	0.0022
0.2248	0.0290	0.126	0.003	0.01	0.2415	0.017
0.4423	0.0616	0.240	0.006	0.02	0.4554	0.013
0.7001	0.104	0.360	0.01	0.02	0.6911	0.0090
0.9283	0.149	0.457	0.01	0.02	0.9002	0.028
1.1664	0.203	0.552	0.01	0.02	1.1176	0.049
1.3677	0.268	0.638	0.02	0.02	1.3182	0.050
1.5219	0.340	0.713	0.02	0.02	1.4771	0.045
1.6036	0.406	0.767	0.02	0.01	1.5707	0.033
T = 343.16 K						
0.0705	0.00562	0.0265	0.0008	0.004	0.0707	0.00019
0.2766	0.0236	0.104	0.004	0.01	0.2719	0.0047
0.6117	0.0627	0.244	0.009	0.03	0.6308	0.019
1.1833	0.136	0.431	0.02	0.04	1.1587	0.025
1.5101	0.195	0.539	0.02	0.04	1.5004	0.010
1.7478	0.249	0.615	0.02	0.03	1.7500	0.0022
1.9433	0.310	0.684	0.02	0.02	1.9616	0.018

U(T, k = 2) = 0.003 K, U(P, k = 2) = 0.0001 MPa

Table 13 : Liquid-vapor data of HFO-1336mzz(Z) – SE 220 at 333K and 383K.

Experimental data					Calculated data	
P_{exp} *MPa*	$w_{ref, exp}$	$x_{ref, exp}$	u(w, k = 2)	u(x, k = 2)	P_{calc} *MPa*	ΔP *MPa*
T = 333.02 K						
0.0694	0.0897	0.248	0.001	0.003	0.0695	0.000090
0.1516	0.245	0.520	0.004	0.005	0.1502	0.0015
0.2063	0.403	0.709	0.006	0.005	0.2085	0.0023
0.2299	0.570	0.816	0.008	0.005	0.2310	0.0010
0.2405	0.682	0.878	0.008	0.004	0.2362	0.0042
T = 383.01 K						
0.2019	0.0776	0.220	0.003	0.007	0.2024	0.00049
0.4691	0.220	0.487	0.007	0.009	0.4712	0.0021
0.6895	0.395	0.686	0.008	0.007	0.6961	0.0066
0.8060	0.578	0.821	0.01	0.006	0.8107	0.0047
0.8408	0.687	0.881	0.009	0.004	0.8350	0.0058

U(T, k = 2) = 0.003 K, U(P, k = 2) = 0.0001 MPa

Table 14 : Liquid-vapor data of HCFO-1233zd(E) – SE 220 at 333K and 383K.

Experimental data					Calculated data	
P_{exp} *MPa*	$w_{ref, exp}$	$x_{ref, exp}$	u(w, k = 2)	u(x, k = 2)	P_{calc} *MPa*	ΔP *MPa*
T = 332.96K						
0.0762	0.0893	0.292	0.001	0.003	0.0821	0.0059
0.1728	0.225	0.550	0.004	0.005	0.1629	0.0099
0.2683	0.396	0.734	0.007	0.006	0.2537	0.015
0.3358	0.568	0.847	0.01	0.006	0.3262	0.0095
0.3752	0.706	0.910	0.01	0.005	0.3611	0.014
T = 382.92 K						
0.2418	0.0732	0.250	0.003	0.008	0.2418	0.000011
0.5376	0.211	0.530	0.006	0.009	0.5382	0.00057
0.8350	0.379	0.720	0.009	0.007	0.8332	0.0018
1.0700	0.560	0.843	0.01	0.006	1.0736	0.0036
1.1900	0.708	0.911	0.01	0.005	1.1869	0.0031

U(T, k = 2) = 0.003 K, U(P, k = 2) = 0.0001 MPa

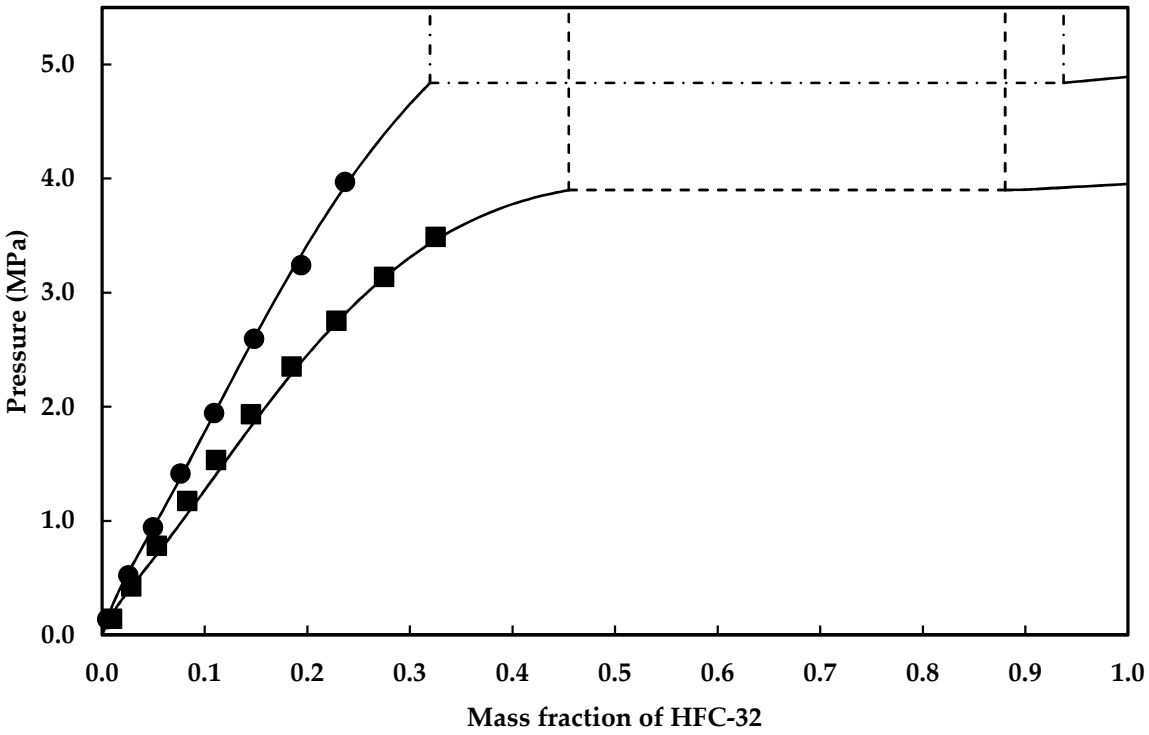

Figure 3 : Phase diagram of HFC-32 – POE 80 at 333K and 343K. ■ : 333K, ● : 343K, lines : model, dashed : liquid-liquid equilibrium.

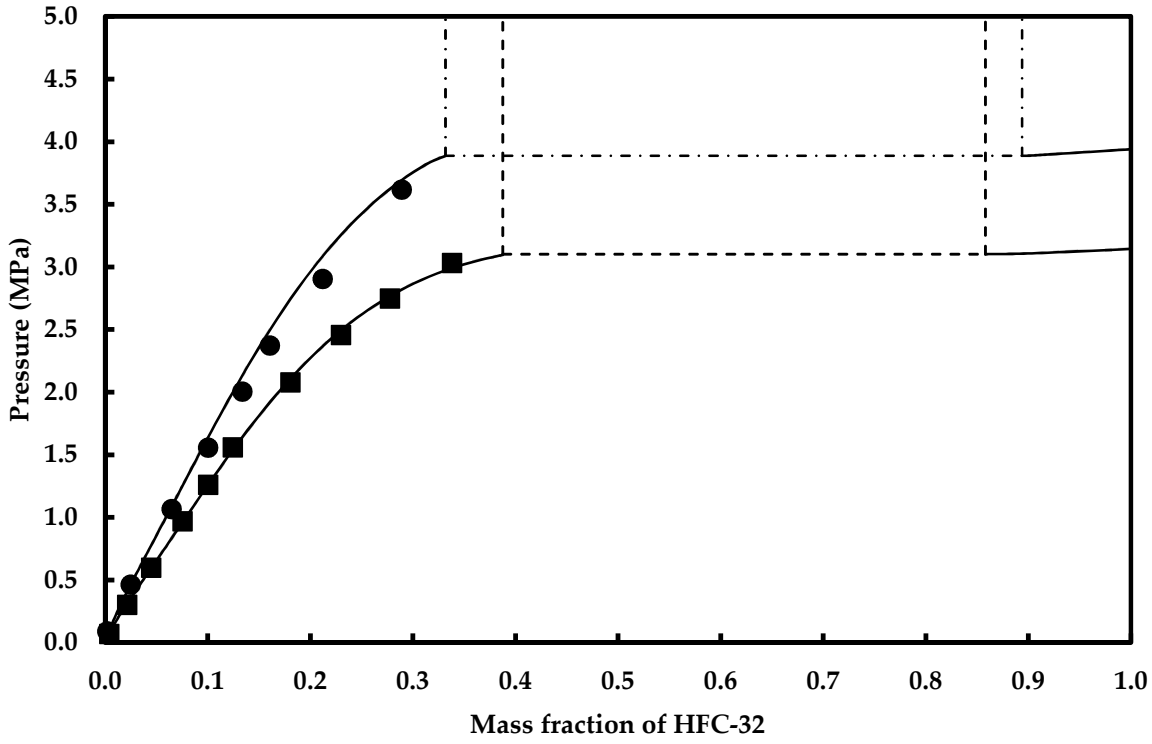

Figure 4 : Phase diagram of HFC-32 – SE 55 at 323K and 333K. ■ : 323K, ● : 333K, lines : model, dashed : liquid-liquid equilibrium.

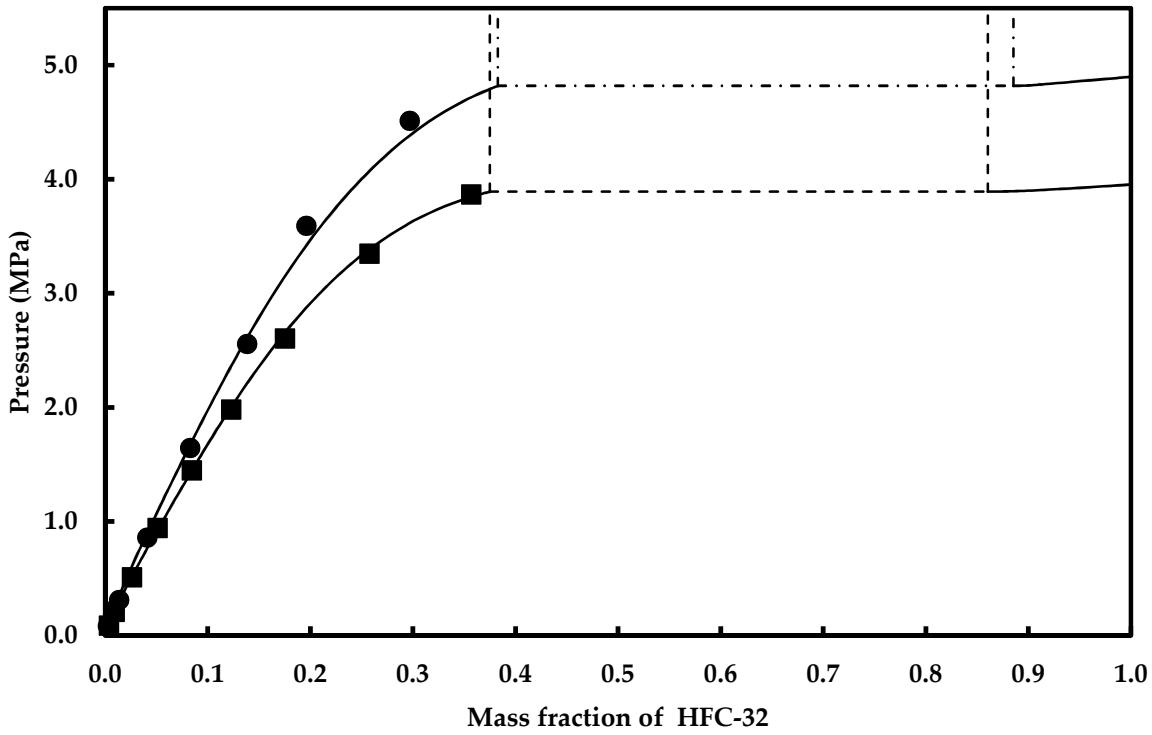

Figure 5 : Phase diagram of HFC-32 – SE 170 at 333K and 343K. ■ : 333K, ● : 343K, lines : model, dashed : liquid-liquid equilibrium.

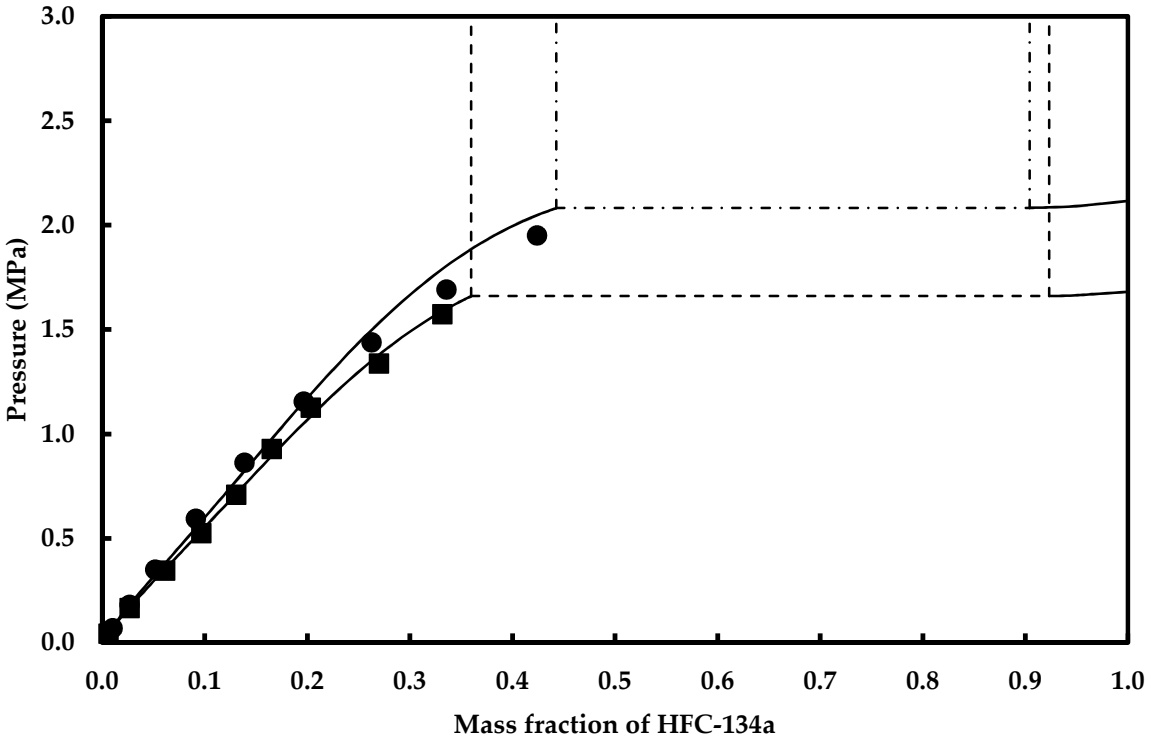

Figure 6 : Phase diagram of HFC-134a – POE 80 at 333K and 343K. ■ : 333K, ● : 343K, lines : model, dashed : liquid-liquid equilibrium.

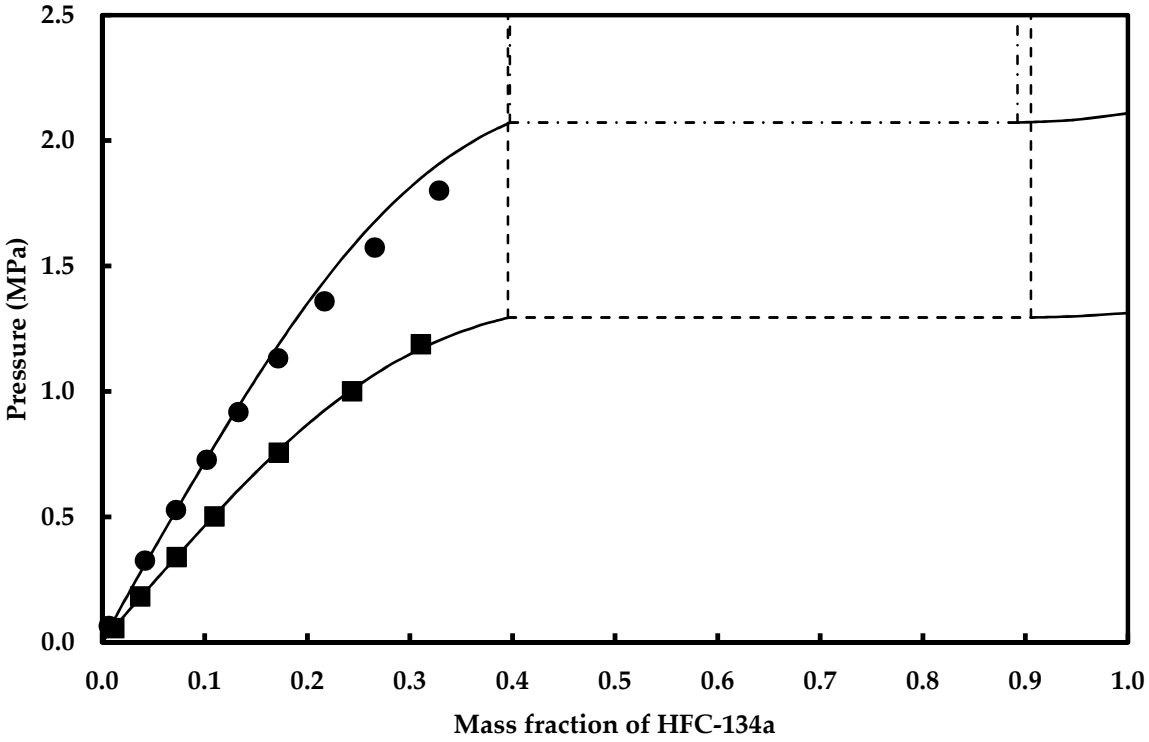

Figure 7 : Phase diagram of HFC-134a – SE 55 at 323K and 343K. ■ : 323K, ● : 343K, lines : model, dashed : liquid-liquid equilibrium.

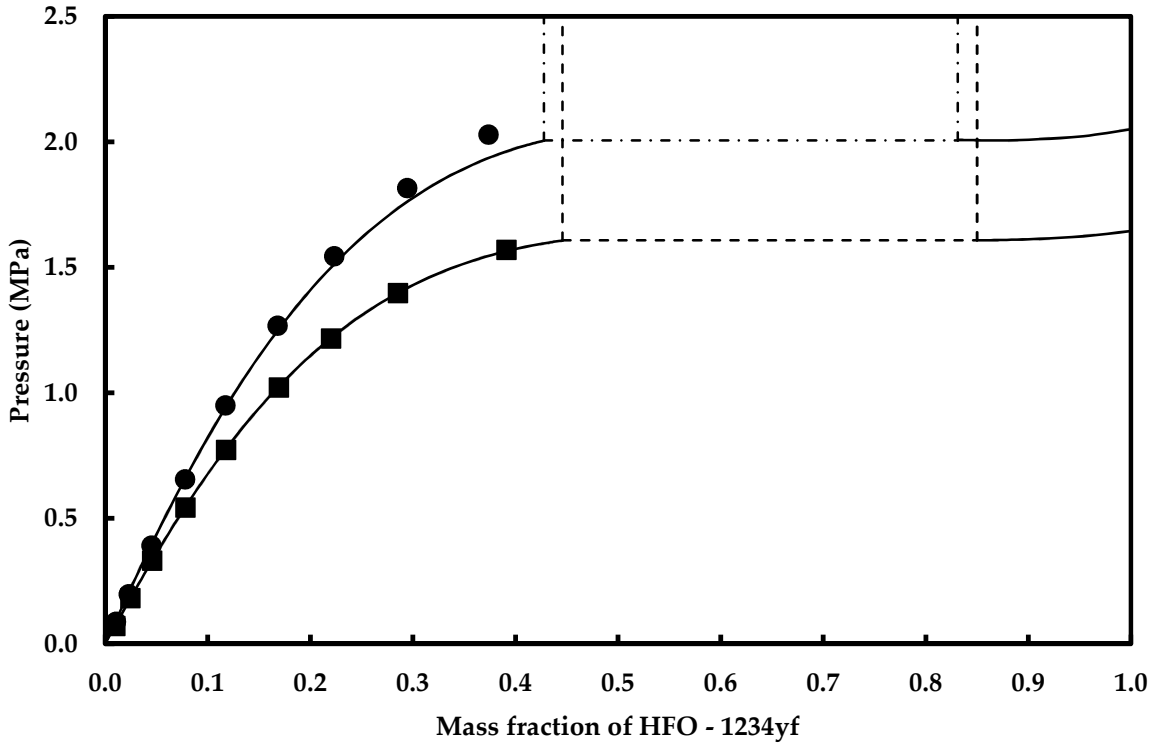

Figure 8 : Phase diagram of HFO-1234yf – POE 80 at 333K and 343K. ■ : 333K, ● : 343K, lines : model, dashed : liquid-liquid equilibrium.

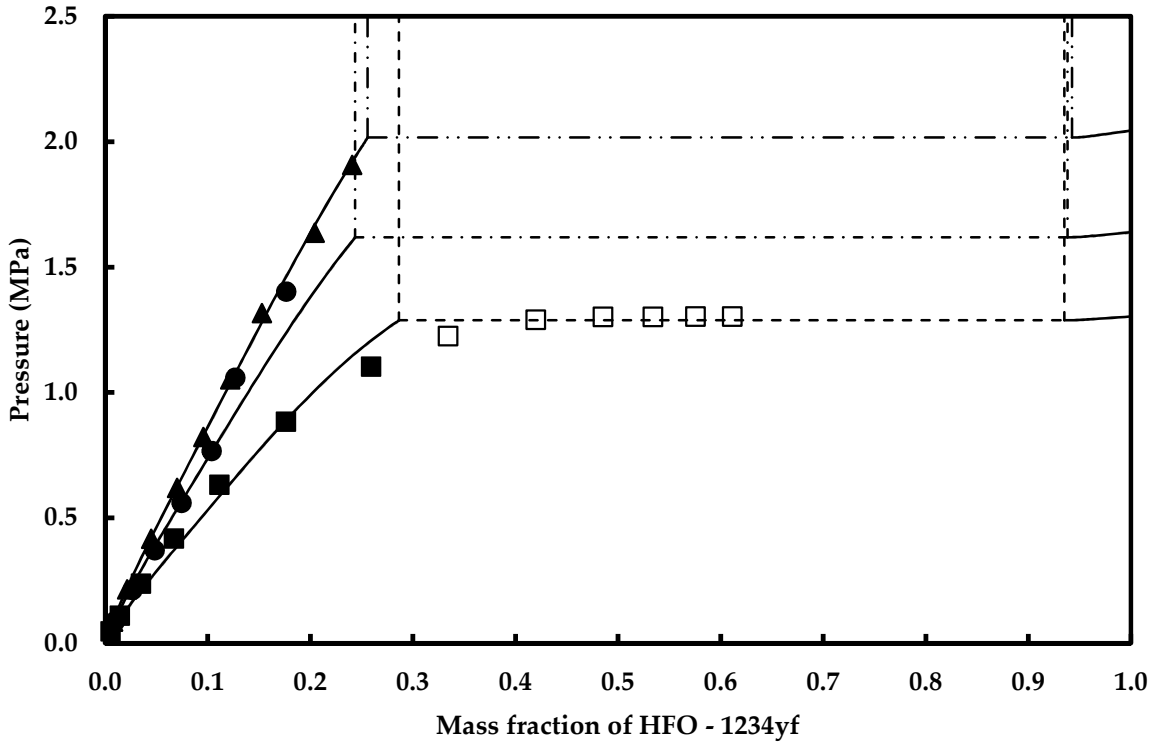

Figure 9 : Phase diagram of HFO-1234yf – SE 55 at 323K, 333K and 343K. ■ : 323K, ● : 333K, ▲ : 343K, lines : model, dashed : liquid-liquid equilibrium, □: questionable measurements.

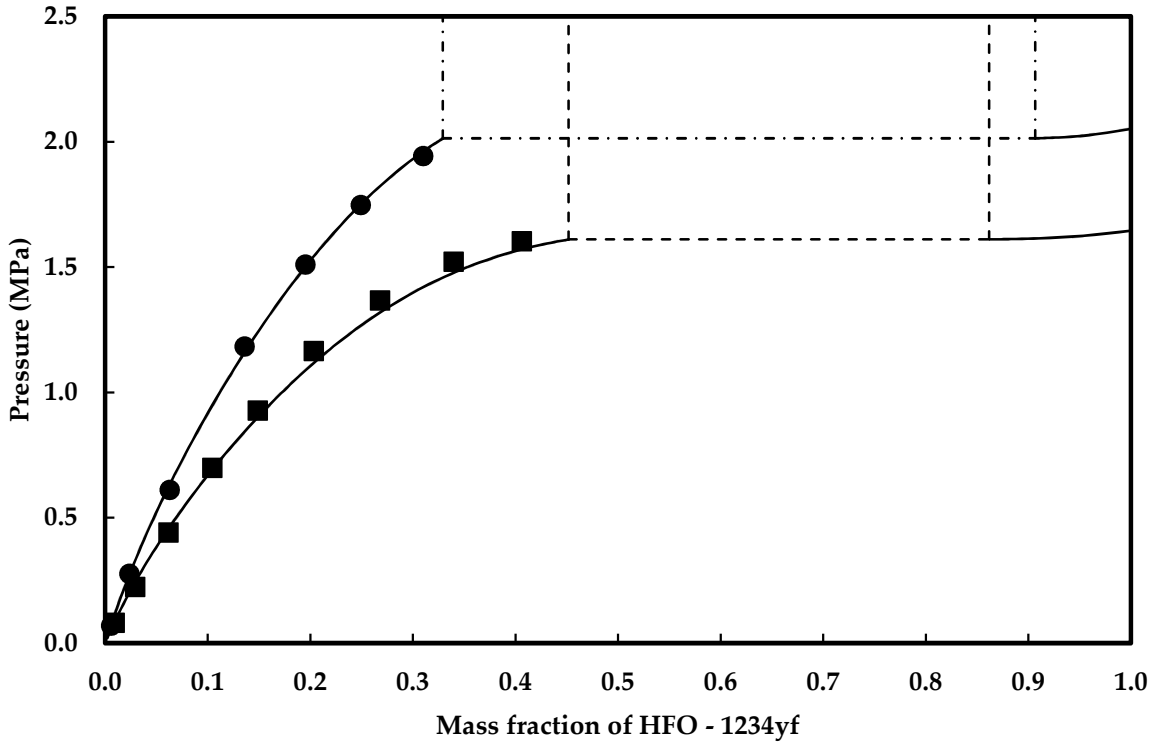

Figure 10 : Phase diagram of HFO-1234yf – SE 170 at 333K and 343K. ■ : 333K, ● : 343K, lines : model, dashed : liquid-liquid equilibrium.

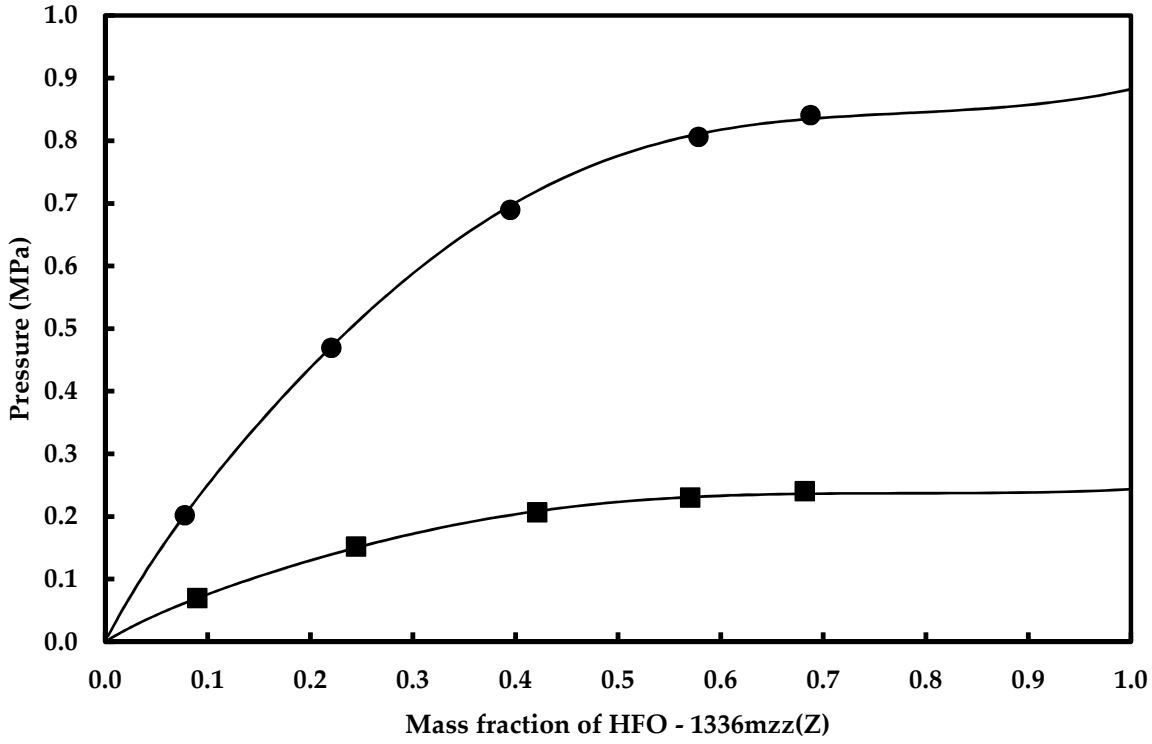

Figure 11 : Phase diagram of HFO-1336mzz(Z) – SE 220 at 333K and 383K. ■ : 333K, ● : 383K, lines : model.

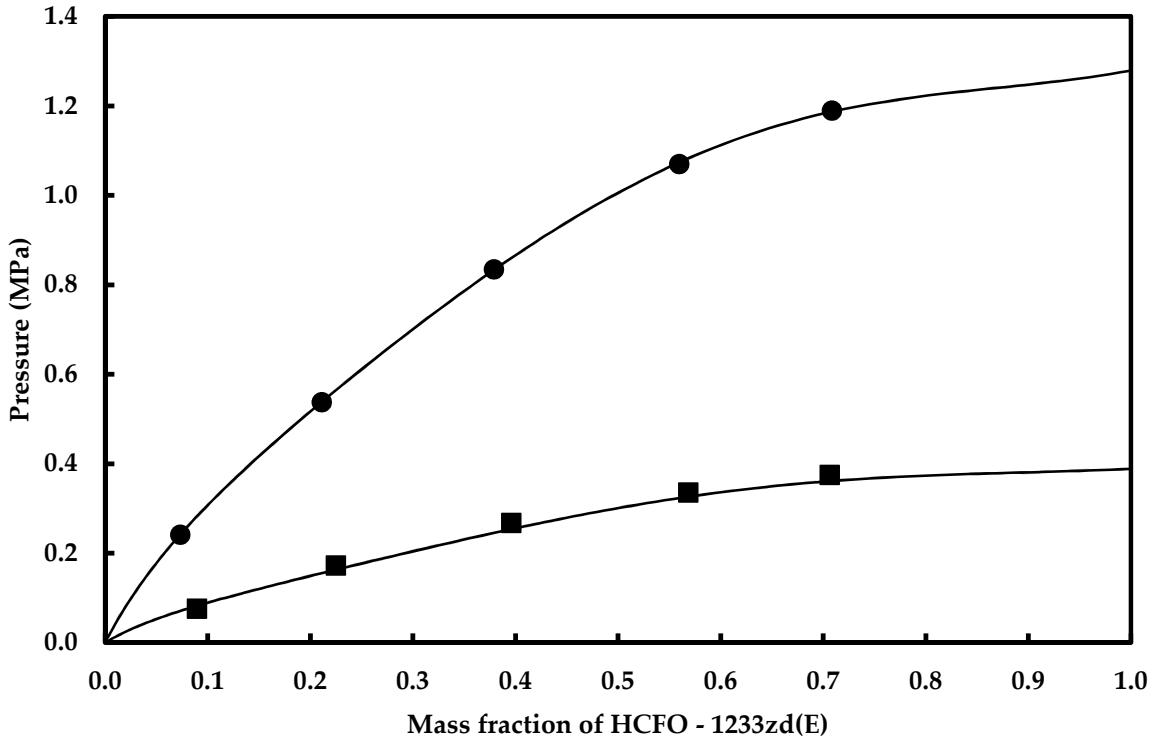

Figure 12 : Phase diagram of HCFO-1233zd(E) – SE 220 at 333K and 383K. ■ : 333K, ● : 383K, lines : model.

Table 15: Binary interaction parameters of refrigerant-lubricant mixtures.

System	T *K*	m_{ij} /	l_{ij} /	l_{ji} /	f_{ij} /	AAD %	BIAS %
			HFC-32				
POE 80	333.15	-0.181874	0.234861	0.161175	1.19015	6.5	-1.3
	343.15	-0.181874	0.234861	0.161175	1.14781	2.1	0.15
SE 55	323.15	-0.361875	0.318459	0.276185	1.33409	1.4	-0.037
	333.15	-0.361875	0.318459	0.276185	1.31352	9.0	-2.3
SE 170	333.15	-0.233339	0.2377	0.198452	1.19241	1.2	0.20
	343.15	-0.233339	0.2377	0.198452	1.19581	4.7	0.20
			HFC-134a				
POE 80	333.15	-0.258846	0.262202	0.218284	1.18712	1.9	-0.048
	343.15	-0.258846	0.262202	0.218284	1.21448	4.7	0.10
SE 55	323.15	-0.236461	0.230715	0.20899	1.17369	1.3	-0.060
	343.15	-0.236461	0.230715	0.20899	1.16923	6.0	-0.30
			HFO-1234yf				
POE 80	333.15	0.228061	-0.281962	-0.280019	0.730128	0.40	-0.010
	343.15	0.228061	-0.281962	-0.280019	0.728873	3.0	-0.30
SE 55	323.15	0.178809	-0.161294	-0.207419	0.759457	12	2.0
	333.15	0.178809	-0.161294	-0.207419	0.743211	5.9	-1.4
	343.15	0.178809	-0.161294	-0.207419	0.746341	1.4	-0.030
SE 170	333.15	-0.25824	0.217829	0.203375	1.19036	3.3	-0.45
	343.15	-0.25824	0.217829	0.203375	1.16462	1.3	0.0063
			HFO-1336mzz(Z)				
SE 220	333.15	-0.0390909	0.0823781	0.0410224	1.00136	0.88	-0.22
	383.15	-0.0390909	0.0823781	0.0410224	0.996853	0.58	0.31
			HCFO-1233zd(E)				
SE 220	333.15	-0.0322544	0.104425	0.0218645	1.05948	5.1	-2.0
	383.15	-0.0322544	0.104425	0.0218645	1.0422	0.18	-0.0076

5. Discussions

All of the mixtures studied in this work are classified as type III systems according to the classification of (Konynenburg and Scott, 1980). In particular, because of the high difference in size between refrigerant and oil molecules, the dew curve is nearly vertical around the pure composition of refrigerant, and horizontal at very low pressures (Quiñones-Cisneros, 1997). In order to discuss the shape of the phase diagrams obtained, we can use a simple γ-ϕ model, defined by equations (25) to (31). The refrigerant-oil mixtures are better assimilated by the phase diagrams shown in Figure 13.

$$Py_i = \gamma_i x_i P_i^{sat} \quad (25)$$

$$Py_{ref} = \gamma_{ref} x_{ref} P_{ref}^{sat} \quad (26)$$

$$Py_{oil} = \gamma_{oil} x_{oil} P_{oil}^{sat} \quad (27)$$

$$K = \frac{P_{ref}^{sat}}{P_{oil}^{sat}} \quad (28)$$

$$G^E = x_{ref} x_{oil} A \quad (29)$$

$$RT \ln(\gamma_{ref}) = A x_{oil}^2 \quad (30)$$

$$RT \ln(\gamma_{oil}) = A x_{ref}^2 \quad (31)$$

Where K is an indicator of size difference between refrigerant and oil molecules and A is an indicator of non-ideality of the mixture formed (the highest the value of A, the stronger the positive deviation from Raoult's law is).

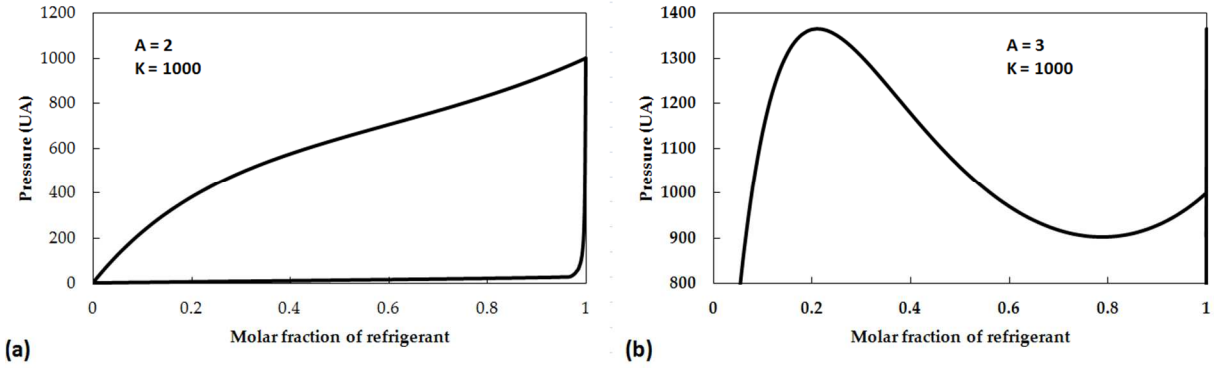

Figure 13 : Examples of phase diagram of binary mixtures. K from equation 28 and A from equation 29.

Phase diagram (a) is representative of the mixture formed by HFO-1336mzz(Z) and HCFO-1233zd(E) with the SE 220 oil. Phase diagram (b) shows an instability of the liquid phase which means the presence of a second liquid phase (liquid-liquid equilibrium). This diagram is coherent with the phase diagram predicted for the mixtures formed by HFC-32, HFC-134 and HFO-1234yf with POE 80, SE 55 and SE 170 oils.

In both cases, the main contribution the the non-ideality of the mixture is the difference of size between the two components (refrigerant and oil). This seems to justify the use of Yokozeki's mixing rule. However, due to the presence of a second liquid phase, it is possible that the mixing rules do not allow an accurate representation of phase equilibrium properties in both liquid-vapor and liquid-liquid regions, as it requires numerous binary interaction parameters.

Also, concerning the modeling results, we have tried to keep m_{ij}, l_{ij} and l_{ji} constants for the same refrigerant – lubricant binary system and to only adjust the f_{ij} parameter with temperature. For some mixtures, this adjustment method do not give good results considering the high deviation results obtained. An optimization of binary interaction parameters for each temperature and each binary produce much more accurate results. This means that some or all of the m_{ij}, l_{ij} and l_{ji} parameters could be temperature dependent and probably the mixture rule considered in this work should be improved or changed.

Experimental work has shown that it can sometimes be difficult to distinguish liquid-liquid phenomenon. As a consequence, some measurements can be uncertain (Figure 9). Moreover, apparition of a second liquid phase could cause the obstruction of the tubing connection between the equilibrium cell and the pressure transducer, leading to a constant pressure although the refrigerant quantity is increased. It is also possible that we did not see the liquid-liquid-equilibrium because the

refractive indexes of both liquid phases are too close to each other. Though no liquid-liquid-vapor equilibrium measurements have been made, liquid-liquid-vapor split have been observed in several occasions (Figure 14). It is noticeable that the heavier liquid phase is, in fact, the oil-rich phase, which shows probable barotropic inversion as explained by (E. Quiñones-Cisneros, 2004) and observed by (Hauk and Weidner, 2000).

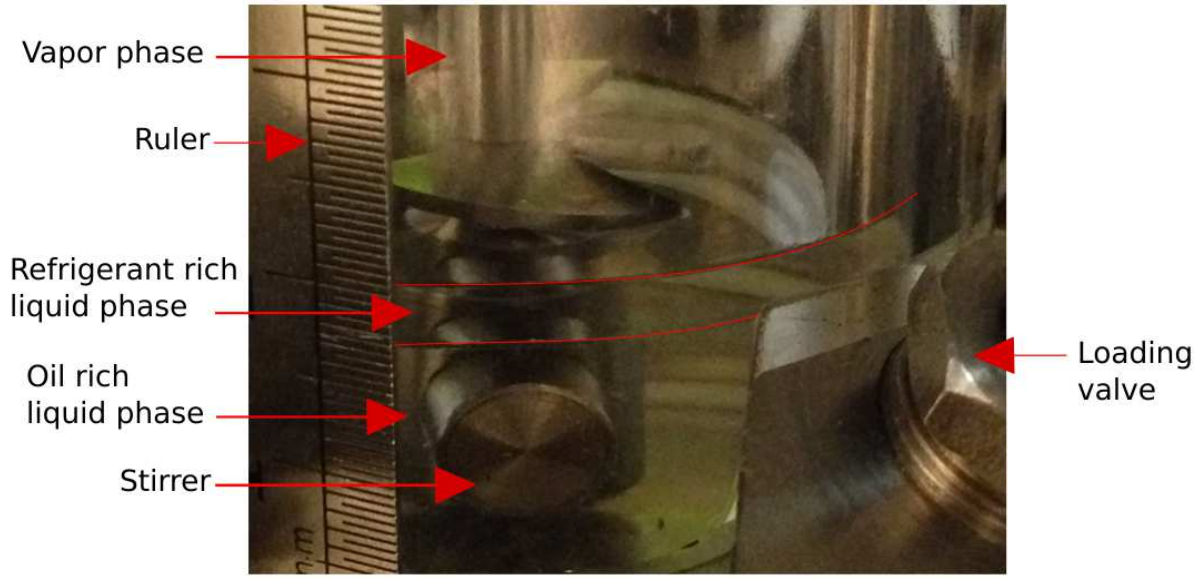

Figure 14 : Picture of liquid-liquid-vapor equilibrium of the HFO-1234yf – SE 55 binary system at 333K.

6. Conclusions

In this work vapor-liquid data of refrigerant-lubricant mixtures were successfully correlated using Yokozeki's model. Tough, if the goal is to be able to extrapolate data to other temperatures, it could be interesting to try to correlate all of the binary interaction parameters to temperature and molecular parameters. Though kinematic viscosity measurements are needed to complete the Daniel plot, one can discard some lubricants on the vapor-liquid equilibrium data only. A lubricant forming liquid-liquid equilibria in the temperature and pressure conditions of a specific system should be avoided. Should one investigate kinematic viscosity modeling of refrigerant-oil lubricant systems, Eyring (Glasstone et al., 1941) provides a model based on activation energy, similar to the Arrhenius equation. This energy can be calculated by an equations of state, like the one used in this work, as demonstrated by the work of (Macías-Salinas et al., 2009), thus making a modeling package fit to obtain Daniel plots.

7. Acknowledgement

The authors are grateful to Fuchs and particularly to Denis Ebert for the Fuchs oil samples. We are also grateful to the ANRT for financing part of this work through the CIFRE fellowship granted to Julien Brocus.

References

Baehr, H.D., Tillner-Roth, R., 1991. Measurement and correlation of the vapour pressures of 1,1,1,2-tetrafluoroethane (R 134a) and of 1,1-difluoroethane (R 152a). The Journal of Chemical Thermodynamics 23, 1063–1068.
Bobbo, S., Zilio, C., Scattolini, M., Fedele, L., 2014. R1234yf as a substitute of R134a in automotive air conditioning. Solubility measurements in two commercial PAG oils. International Journal of Refrigeration 40, 302–308.
Coquelet, C., Chapoy, A., Richon, D., 2004. Development of a New Alpha Function for the Peng–Robinson Equation of State: Comparative Study of Alpha Function Models for Pure Gases (Natural Gas Components) and Water-Gas Systems. International Journal of Thermophysics 25, 133–158.
Dang, C., Hoshika, K., Hihara, E., 2012. Effect of lubricating oil on the flow and heat-transfer characteristics of supercritical carbon dioxide. International Journal of Refrigeration 35, 1410–1417.
Daniel, G., Anderson, M.J., Schmid, W., Tokumitsu, M., 1982. Performance of selected synthetic lubricants in industrial heat pumps. Journal of Heat Recovery Systems 2, 359–368.
Descamps, C., Coquelet, C., Bouallou, C., Richon, D., 2005. Solubility of hydrogen in methanol at temperatures from 248.41 to 308.20K. Thermochimica Acta 430, 1–7.
E. Quiñones-Cisneros, S., 2004. Barotropic phenomena in complex phase behaviour. Physical Chemistry Chemical Physics 6, 2307–2313.
Glasstone, S., Laidler, K.J., Eyring, H., 1941. The Theory of Rate Processes: The Kinetics of Chemical Reactions, Viscosity, Diffusion and Electrochemical Phenomena. McGraw-Hill Book Company, Incorporated.
Guide to the Expression of Uncertainty in Measurement (No. JCGM 100:2008), 2008.
Hauk, A., Weidner, E., 2000. Thermodynamic and Fluid-Dynamic Properties of Carbon Dioxide with Different Lubricants in Cooling Circuits for Automobile Application. Ind. Eng. Chem. Res. 39, 4646–4651.
Jia, T., Bi, S., Wu, J., Jiang, W., Li, P., 2021. Experimental investigation for the solubilities of 2,3,3,3-tetrafluoroprop-1-ene (R1234yf) in polyol ester, polyvinylether, and polyalkylene glycol base oils. International Journal of Refrigeration 125, 84–89.
Jia, X., Wang, J., Wang, X., Hu, Y., Sun, Y., 2020. Phase equilibrium of R1234yf and R1234ze(E) with POE lubricant and thermodynamic performance on the evaporator. Fluid Phase Equilibria 514, 112562.
Konynenburg, P.H. van, Scott, R.L., 1980. Critical lines and phase equilibria in binary van der Waals mixtures. Phil. Trans. R. Soc. Lond. A 298, 495–540.
Kruse, H.H., Schroeder, M., 1985. Fundamentals of lubrication in refrigerating systems and heat pumps. International Journal of Refrigeration 8, 347–355.
Le Guennec, Y., Lasala, S., Privat, R., Jaubert, J.-N., 2016. A consistency test for α-functions of cubic equations of state. Fluid Phase Equilibria.
Lemmon, E.W., Bell, I.H., Huber, M.L., 2018. NIST Standard Reference Database 23: Reference Fluid Thermodyamic and Transport Properties -REFPROP, version 10.0, National Institute of Standards and Technology.
Liu, L., Chen, S., 1996. Correlation of the Acentric Factor for Hydrocarbons. Ind. Eng. Chem. Res. 35, 2484–2486.
Macías-Salinas, R., Durán-Valencia, C., López-Ramírez, S., Bouchot, C., 2009. Eyring-Theory-Based Model To Estimate Crude Oil Viscosity at Reservoir Conditions. Energy Fuels 23, 464–470.
Malbrunot, P.F., Meunier, P.A., Scatena, G.M., Mears, W.H., Murphy, K.Paul., Sinka, J.V., 1968. Pressure-volume-temperature behavior of difluoromethane. J. Chem. Eng. Data 13, 16–21.
Mang, Dresel, W., 2007. Lubricants and Lubrication. John Wiley & Sons.
Marcelino Neto, M.A., França, R.M., Barbosa, J.R., 2014. Convection-driven absorption of R-1234yf in lubricating oil. International Journal of Refrigeration 44, 151–160.
Marsh, K.N., Kandil, M.E., 2002. Review of thermodynamic properties of refrigerants + lubricant oils. Fluid Phase Equilibria, 2nd international workshop on thermochemical, thermodynamic and transport properties of halogenated hydrocarbons and mixtures 199, 319–334.

Mondéjar, M.E., McLinden, M.O., Lemmon, E.W., 2015. Thermodynamic Properties of trans-1-Chloro-3,3,3-trifluoropropene (R1233zd(E)): Vapor Pressure, (p, ρ, T) Behavior, and Speed of Sound Measurements, and Equation of State. J. Chem. Eng. Data 60, 2477–2489.
Morais, A.R.C., Simoni, L.D., Scurto, A.M., Shiflett, M.B., 2020. Solubility and Diffusivity of Hydrofluoroolefin Refrigerants in a Polyol Ester Lubricant. Ind. Eng. Chem. Res. 59, 6279–6287.
Nelder, J.A., Mead, R., 1965. A Simplex Method for Function Minimization. Comput J 7, 308–313.
Quiñones-Cisneros, S.E., 1997. Phase and critical behavior in type III phase diagrams. Fluid Phase Equilibria 134, 103–112.
Quiñones-Cisneros, S.E., García, J., Fernández, J., Monsalvo, M.A., 2005. Phase and viscosity behaviour of refrigerant–lubricant mixtures. International Journal of Refrigeration 28, 714–724.
Redlich, O., Kwong, J.N.S., 1949. On the thermodynamics of solutions; an equation of state; fugacities of gaseous solutions. Chem Rev 44, 233–244.
Richter, M., McLinden, M.O., Lemmon, E.W., 2011. Thermodynamic Properties of 2,3,3,3-Tetrafluoroprop-1-ene (R1234yf): Vapor Pressure and p–ρ–T Measurements and an Equation of State. J. Chem. Eng. Data 56, 3254–3264.
Seeton, C.J., 2006. Viscosity–temperature correlation for liquids. Tribol Lett 22, 67–78.
Soave, G., 1972. Equilibrium constants from a modified Redlich-Kwong equation of state. Chemical Engineering Science 27, 1197–1203.
Sun, Y., Di, G., Wang, J., Wang, X., He, M., 2020. Phase behavior of R1234yf and R600a in pentaerythritol tetranonanoate. International Journal of Refrigeration 109, 135–142.
Sun, Y., Wang, X., Wang, D., Jin, L., 2017. Measurement and correlation for phase equilibrium of HFO1234yf with three pentaerythritol esters from 293.15K to 348.15K. The Journal of Chemical Thermodynamics 112, 122–128.
Tanaka, K., Akasaka, R., Sakaue, E., Ishikawa, J., Kontomaris, K.K., 2016. Thermodynamic Properties of cis-1,1,1,4,4,4-Hexafluoro-2-butene (HFO-1336mzz(Z)): Measurements of the pρT Property and Determinations of Vapor Pressures, Saturated Liquid and Vapor Densities, and Critical Parameters. J. Chem. Eng. Data 61, 2467–2473.
van de Bor, D.M., Infante Ferreira, C.A., Kiss, A.A., 2015. Low grade waste heat recovery using heat pumps and power cycles. Energy 89, 864–873.
Wang, X., Sun, Y., Gong, N., 2016. Experimental investigations for the phase equilibrium of R1234yf and R1234ze(E) with two linear chained pentaerythritol esters. The Journal of Chemical Thermodynamics 92, 66–71.
Yokozeki, A., 2007. Solubility correlation and phase behaviors of carbon dioxide and lubricant oil mixtures. Applied Energy 84, 159–175.
Yokozeki, A., 2001. Solubility of Refrigerants in Various Lubricants. International Journal of Thermophysics 22, 1057–1071.
Youbi-Idrissi, M., Bonjour, J., 2008. The effect of oil in refrigeration: Current research issues and critical review of thermodynamic aspects. International Journal of Refrigeration 31, 165–179.
Zhang, F., Théveneau, P., El Ahmar, E., Canet, X., Soo, C.-B., Coquelet, C., 2016. An improved static–analytic apparatus for vapor–liquid equilibrium (PTxy) measurement using modified in-situ samplers. Fluid Phase Equilibria 409, 425–433.

8. Appendix

The composed uncertainty of the molar fraction of refrigerant in the liquid phase is calculated using:

$$u_c(x_i) = \sqrt{\left(\frac{\partial x_i}{\partial w_i}\right)^2 u_c^2(w_i) + \left(\frac{\partial x_i}{\partial M_i}\right)^2 u^2(M_i) + \left(\frac{\partial x_i}{\partial M_j}\right)^2 u^2(M_j)} \quad \text{(I-1)}$$

With the following partial derivatives:

$$\left(\frac{\partial x_i}{\partial w_i}\right) = \frac{M_i M_j}{\left(M_i w_i - M_j w_i - M_i\right)^2} \quad \text{(I-2)}$$

$$\left(\frac{\partial x_i}{\partial M_i}\right) = \frac{w_i M_j (w_i - 1)}{\left(M_i w_i - M_j w_i - M_i\right)^2} \quad \text{(I-3)}$$

$$\left(\frac{\partial x_i}{\partial M_j}\right) = \frac{w_i (1 - w_i)}{M_i M_j^2 \left(\frac{w_i}{M_i} + \frac{1 + w_i}{M_j}\right)^2} \quad \text{(I-4)}$$

The composed uncertainty on the mass fraction of refrigerant in the liquid phase is calculated with:

$$u_c(w_i) = \sqrt{\left(\frac{\partial w_i}{\partial m_i^{tot}}\right)^2 u(m_i^{tot})^2 + \left(\frac{\partial w_i}{\partial m_i^{vap}}\right)^2 u(m_i^{vap})^2 + \left(\frac{\partial w_i}{\partial m_{huile}}\right)^2 u(m_{huile})^2} \quad \text{(I-5)}$$

With the following partial derivatives:

$$\left(\frac{\partial x_i}{\partial m_i^{tot}}\right) = \frac{m_{huile}}{\left(m_i^{tot} - m_i^{vap} + m_{huile}\right)^2} \quad \text{(I-6)}$$

$$\left(\frac{\partial x_i}{\partial m_i^{vap}}\right) = \frac{-m_{huile}}{\left(m_i^{tot} - m_i^{vap} + m_{huile}\right)^2} \quad \text{(I-7)}$$

$$\left(\frac{\partial x_i}{\partial m_i^{vap}}\right) = \frac{-\left(m_i^{tot} - m_i^{vap}\right)}{\left(m_i^{tot} - m_i^{vap} + m_{huile}\right)^2} \quad \text{(I-8)}$$

While the composed uncertainty of the total mass of refrigerant and oil introduced in the equilibrium cell is calculated with:

$$u_c(m) = \sqrt{\left(\frac{\partial m}{\partial V}\right)^2 u(V)^2 + \left(\frac{\partial m}{\partial \rho}\right)^2 u(\rho)^2} \quad \text{(I-9)}$$

With the following partial derivatives:

$$\left(\frac{\partial m}{\partial V}\right) = \rho \quad \text{(I-10)}$$

$$\left(\frac{\partial m}{\partial \rho}\right) = V \quad \text{(I-11)}$$

With the uncertainty of the volume displaced by the piston of the variable volume cell is:

$$u_c(V) = \sqrt{\left(\frac{\partial V}{\partial D}\right)^2 u(D)^2 + \left(\frac{\partial V}{\partial l_f}\right)^2 u(l_f)^2 \left(\frac{\partial V}{\partial l_i}\right)^2 u(l_i)^2} \quad \text{(I-12)}$$

With the following partial derivatives:

$$\left(\frac{\partial V}{\partial D}\right) = \frac{\pi D}{2}\left(l_f - l_i\right) \quad \text{(I-13)}$$

$$\left(\frac{\partial V}{\partial l_f}\right) = \frac{\pi D^2}{4} \quad \text{(I-14)}$$

$$\left(\frac{\partial V}{\partial l_i}\right) = -\frac{\pi D^2}{4} \quad \text{(I-15)}$$

With the following standard uncertainties:

$$u(l_f, l_i) = 0.0003\ cm \quad \text{(I-16)}$$

$$u(D) = 0.006\ cm \quad \text{(I-17)}$$

The uncertainty of the residual mass of refrigerant in the vapor phase is computed with the equation (I-9), with the uncertainty on the vapor volume:

$$u_c(V) = \sqrt{\left(\frac{\partial V}{\partial V_{cell}}\right)^2 u(V_{cell})^2 + \left(\frac{\partial V}{\partial D}\right)^2 u(D)^2 \left(\frac{\partial V}{\partial h}\right)^2 u(h)^2} \quad \text{(I-18)}$$

With the following partial derivatives:

$$\left(\frac{\partial V}{\partial h}\right) = \frac{\pi D^2}{4} \quad \text{(I-19)}$$

$$\left(\frac{\partial V}{\partial D}\right) = \frac{\pi D}{2} h \quad \text{(I-20)}$$

With the following standard uncertainties:

$$u(V_{cell}) = 4\% \quad \text{(I-21)}$$

$$u(D) = 0.006 \text{ cm} \quad \text{(I-22)}$$

$$u(h) = 0.01\ cm \quad \text{(I-23)}$$

While it is difficult to evaluate the purity of the oil used, it is fitting to add the uncertainty associated with the purity of the refrigerants used:

$$u_{pureté} = \frac{1-p}{\sqrt{3}} \quad \text{(I-24)}$$

With *p*, the purity of the refrigerant.